

## Ferroelectric switching by the grounded scanning probe microscopy tip

A. V. Ievlev,<sup>1,2,\*</sup> A. N. Morozovska,<sup>3</sup> V. Ya. Shur,<sup>4</sup> and S. V. Kalinin<sup>1,2</sup>

<sup>1</sup>The Institute for Functional Imaging of Materials, Oak Ridge National Laboratory, One Bethel Valley Rd., Oak Ridge, Tennessee 37831, USA

<sup>2</sup>The Center for Nanophase Materials Sciences, Oak Ridge National Laboratory, One Bethel Valley Rd., Oak Ridge, Tennessee 37831, USA

<sup>3</sup>Institute of Physics, National Academy of Sciences of Ukraine, 46, pr. Nauki, 03028 Kyiv, Ukraine

<sup>4</sup>Ferroelectric Laboratory, Institute of Natural Sciences, Ural Federal University, 51, Lenin Ave., 620000 Ekaterinburg, Russia

(Received 7 March 2015; revised manuscript received 5 May 2015; published 19 June 2015)

Polarization reversal in ferroelectrics by the tip of a scanning probe microscope (SPM) has been intensively studied over the last two decades. In addition to classical domain formation and growth, a number of abnormal switching phenomena have been reported. In particular, it was experimentally and theoretically shown that slow dynamics of surface screening can control the kinetics of the ferroelectric switching, and result in backswitching and relaxation phenomena. Here we experimentally demonstrate the practical possibility of the history dependent polarization reversal by the grounded SPM tip. This phenomenon was attributed to the induction of the slowly dissipating charges into the surface, which in the presence of the grounded tip induce polarization reversal. Analytical and numerical electrostatic calculations allow additional insight into the mechanisms of the observed phenomena.

DOI: [10.1103/PhysRevB.91.214109](https://doi.org/10.1103/PhysRevB.91.214109)

PACS number(s): 77.84.-s, 77.84.Ek

Piezoresponse force microscopy (PFM) is one of the most popular techniques used for the complex investigations of the ferroelectric materials, allowing visualization of the static ferroelectric domain structures [1–3]. At the same time application of the electric field through a conductive tip opens a pathway for manipulation with the domain structures on the nanoscale [4,5].

The process of polarization reversal under the action of an electric field produced by the SPM tip has been studied by multiple scientific groups [6–20]. Abnormal switching behaviors, including backswitching [12,15,21–23], polarization reversal by the “wrong” polarity of the switching voltage [7,11,17,19], and switching along the path of the unbiased SPM tip [18,24] were reported. These phenomena were attributed to charge injection [12,15], screening of the applied electric fields [25], and ferroelastoelectric switching [7]. Despite clear relevance to the qualitative and quantitative interpretation of PFM-derived data on polarization switching, the exact origins of the observed phenomena remain poorly understood.

Here we experimentally studied the process of the tip-induced polarization reversal in the vicinity of the flat domain wall in the thin periodically poled LiNbO<sub>3</sub> single crystal. Investigations demonstrated unexpected pronounced switching along the path of the grounded SPM tip at distances above 1 μm from the point of the field application. This switching led to the formation of sharp spikes on the initial flat domain wall and nanodomain chains. The obtained results were explained in terms of the spatial distribution of the electric field produced by freshly switched domains and grounded SPM tip. Analytical and numerical calculations of the electric field distribution showed the presence of the pronounced induced electric field into the tip surface. Observed phenomenon allows explanation of a number of the abnormal switching dynamics reported earlier [12,15,18]. However, it gives rise to a much wider set of behaviors. For instance, it enables switching (not

backswitching) by the grounded tip in the completely screened areas.

In addition, interaction with a flat domain wall and formation of the nanodomain chains are experimentally and theoretically considered. Obtained experimental and theoretical results are important for quantitative analysis of the results acquired by all electrical SPM techniques realized on the samples in the presence of the surface and bulk charges.

In the experiments we used a periodically poled plate of the congruent lithium niobate LiNbO<sub>3</sub> single crystal. The sample was thinned down to 20 μm by mechanical polishing. Experiments were performed with commercial scanning probe microscopes Cypher and MFP3D (Asylum Research, USA) using Multi-75G-E SPM tips (Budget Sensors, USA) with a conductive platinum coating and a nominal radius of curvature of the tips  $R_{\text{tip}} < 25$  nm. Local polarization reversal was induced by the electric field produced by the tip using triangular bipolar pulses with amplitude  $U_{\text{sw}} = 20$ –100 V and duration  $t_{\text{sw}} = 250$  ms. The band excitation PFM mode was used for visualization of the resulting domain structures. Experiments were carried out at room conditions: temperature about 23 °C and 30%–40% relative humidity.

The switching process was realized over two-dimensional (2D) arrays of the switching points [Fig. 1(a)] with SPM tip motion in two modes: “contact” and “noncontact.” In the contact mode the tip stayed in contact with the sample surface at all times, while in noncontact mode it was withdrawn from the surface following the application of the switching pulse.

The formed domain structures were found significantly dependent on the used tip motion mode [Figs. 1(b)–1(e) and 2]. The formation of a domain at the points of the voltage application was only observed in the noncontact mode [Figs. 1(b) and 1(c)], while the switching in the contact mode also revealed formation of the nanometer-sized domains along the path of the grounded SPM tip [Figs. 1(d) and 1(e)].

In both modes, polarization switching with formation of the domains has been observed only in the areas of the sample with the spontaneous polarization directed downward

\*Author to whom correspondence should be addressed: [ievlevav@ornl.gov](mailto:ievlevav@ornl.gov)

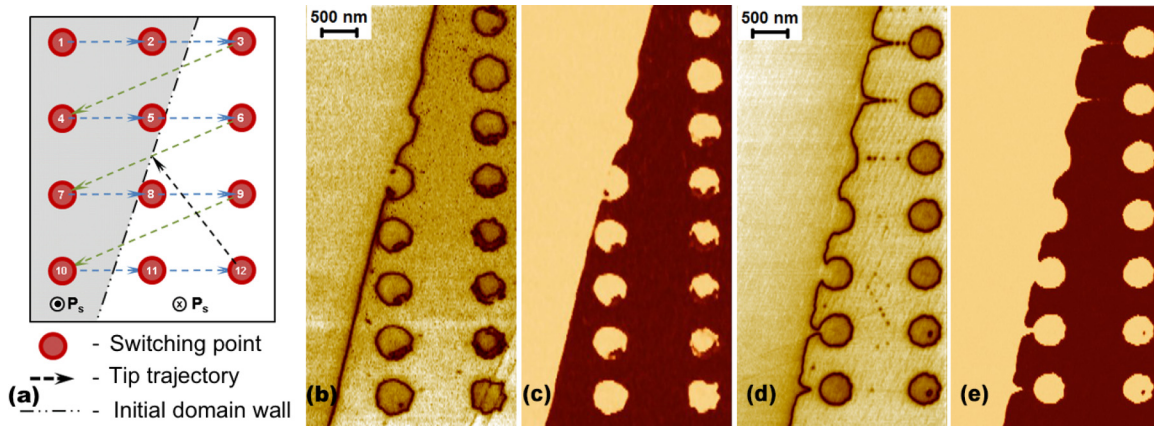


FIG. 1. (Color online) Tip-induced switching in the thin  $\text{LiNbO}_3$  single crystal. (a) Switching scheme. Domain structures formed after switching in (b) and (c) noncontact and (d) and (e) contact tip motion modes. (b) and (d) Amplitude and (c) and (e) phase of the piezoresponse signal.

( $Z^-$  polar surface) [Figs. 1(b)–1(e)]. The formation of the domains on the  $Z^+$  polar surface has not been observed in the used range of the switching voltages. This fact can be explained by the complete backswitching phenomenon which leads to the disappearance of the just formed domains. Anisotropy of the backswitching during tip induced polarization reversal was recently reported on the nonpolar cut of the lithium niobate single crystal [26] and attributed to the different values of the mobility of the screening charges on the sample surface. In the current situation this anisotropy results in a significant difference of the screening efficiency on  $Z^+$  and  $Z^-$  surfaces.

The shape and size of the isolated domains formed on the  $Z^-$  polar surface in the points of the field application was found independent on the mode of the tip motion [Figs. 1(b)–1(e)]. However, a significant difference was revealed along the path of the grounded tip. In the contact mode, it led to the formation of sharp domain spikes on the flat domain wall [Figs. 1(c) and 3(a)] and the nanodomain chains along the tip path [Figs. 1(c) and 3(b)]. This effect was found to be more pronounced at higher amplitudes of the switching pulses (Fig. 2).

The experimental results explicitly demonstrate the possibility of the ferroelectric switching by the nominally grounded SPM tip. However, as we believe this nontrivial phenomenon has a very simple physical explanation. It can be ascribed to the interaction between slow screening charge dynamics (surface and bulk) which can be affected both by the ferroelectric domain state and electrostatics of the tip-surface system.

First, we consider formation of the sharp spike on the initially flat domain wall [Fig. 3(a)]. This phenomenon was observed after switching on the  $Z^+$  polar surface. Although it does not lead to the formation of the stable isolated domain, it changes spatial distribution of the screening charges [27–29] [Fig. 3(c)]. Furthermore, the complete screening of the depolarization electric field in the absence of the top electrode can take seconds [30], which leads to the existence of the uncompensated charge on the surface of the sample. This induces opposite charges in the surface of the grounded SPM tip and leads to the appearance of a highly localized electric field of the same direction as a spontaneous polarization of the unscreened area [Fig. 3(c)]. The motion of the tip into the area of the antiparallel domain ( $Z^-$ ) creates the conditions for

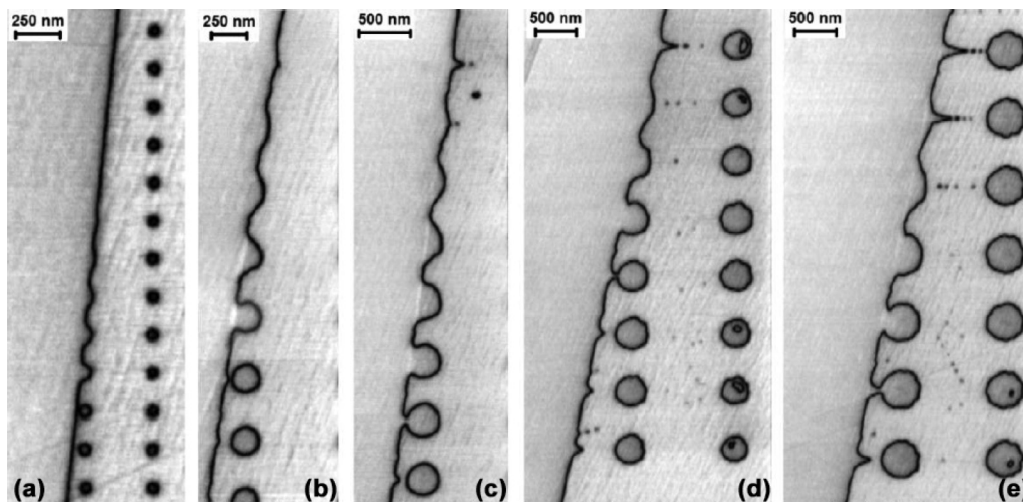


FIG. 2. Tip-induced switching in contact mode in  $\text{LiNbO}_3$  single crystal near the flat domain wall with different amplitudes of the switching pulses: (a) 20 V, (b) 40 V, (c) 60 V, (d) 80 V, and (e) 100 V. PFM amplitude signal.

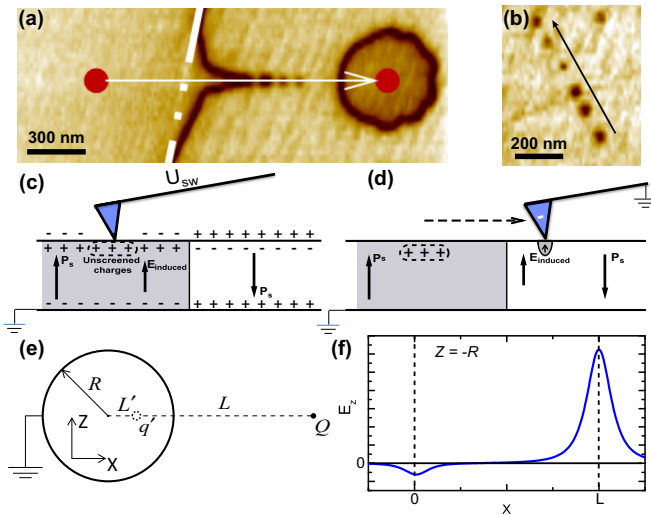


FIG. 3. (Color online) (a) and (b) Detailed PFM amplitude images of the domain structures formed along the path of the grounded tip: (a) spike on the domain wall and (b) nanodomain chain. (c) and (d) Scheme of the switching mechanism. (c) Initial switching and complete backswitching far from the domain wall. (d) Switching under the action of the electric field produced by the induced charges. (e) and (f) Model electrostatic problem: grounded conductive sphere and point charge: (e) scheme and (f) distribution of the  $z$  component of the electric field along the line  $z = -R$ ;  $y = 0$ .

the polarization reversal [Fig. 3(d)] and formation of the new domains.

At the same time, formation of the nanodomain chains cannot be observed between freshly switched isolated domains. In this case spatial distribution of the charges is completely different. Unscreened charges on the sample surface are partially compensated by bulk charges on tail-to-tail domain walls. This is in agreement with recent experimental studies of the backswitching behavior [18], in which case the grounded tip induces back poling inside freshly switched domains, but not formation of new domains outside. This fact has also been experimentally confirmed by multiple switching with different amplitudes of the switching pulses (Fig. 2).

A qualitative picture of the electric field produced by the grounded SPM tip can be derived using a simplified model of the grounded sphere with radius  $R$ , with the center in the point  $(0; 0; 0)$  near the point charge  $Q$  located at distance  $L$  in the point  $(L; 0; 0)$  [Fig. 3(e)]. Analytically an electric field produced by this system can be calculated using a method of the images. Neglecting the influence of the air-ferroelectric boundary on the field distribution, the total electric field can be found as a superposition of the electric field produced by the charge  $Q$  and imaginary charge  $q'$  located in the point  $(0; 0; l')$ , where  $q' = Q \cdot R/L$  and  $l' = R^2/L$ . Thus, the  $z$  component of the resulted electric field along the line  $z = -R$  (analog of the sample surface) have two pronounced maxima [Fig. 3(f)]. The left one represents an electric field produced by charges induced into the sphere, which in the case of the grounded tip is responsible for the observed polarization reversal.

To derive a quantitative description accounting for the finite size of the partially unscreened bound charge located at the domain face near the sample surface, the presence of

the boundary of the two dielectrics (one is anisotropic) and presence of the grounded bottom electrode, not considered above in the toy model, we used the COMSOL Multiphysics package for the solution of the electrostatic equations by the finite elements method. In the simulations the SPM tip was modeled by part of the sphere with radius  $R_{\text{tip}} = 20$  nm and a conical part with angle  $10^\circ$ , oriented normally to the sample surface [Fig. 4(a)]. The sample was modeled as an anisotropic dielectric with a diagonal tensor of the relative permittivity with  $\epsilon_{xx} = \epsilon_{yy} = 84$  and  $\epsilon_{zz} = 35$ . The partially screened charge was modeled as a disk with radius  $R_{\text{ch}} = 100$  nm and the center located at a distance  $\Delta X$  from the tip on the surface of the sample with the surface charge density  $\sigma = 0.05 \cdot P_S = 3.75 \mu\text{C}/\text{m}^2$ , which corresponds to a 95% screened surface of the cylindrical domain with radius  $R_{\text{ch}}$ . The surface of the SPM tip and the bottom electrode were assumed grounded for the simulations.

As expected, the simulations showed that the grounded tip induces a strong electric field spatially localized in the nanometer sized area [Fig. 4(b)]. The maximal value of the electric field decreases when the distance between the tip and the charged disk is increased [Fig. 4(c)]. It should be noted that even at a sufficiently long distance from the charged disk ( $\Delta X = 500$  nm) the value of the tip induced electric field is high enough for polarization reversal.

Detailed simulations showed that the peak value of the  $z$  component of the induced electric field  $E_{\text{peak}}^z$  exceeds the threshold field of the congruent lithium niobate  $E_{\text{th}} = 21$  kV/mm for thick ( $>2.5 \mu\text{m}$ ) plates even at distances above  $1 \mu\text{m}$  [Fig. 5(a)].  $E_{\text{peak}}^z$  was found to be strongly dependent on the sample thickness [Fig. 5(b)]. For example, in the 100-nm-thick sample the induced electric field exceeds  $E_{\text{th}}$  only at  $\Delta X = 250$  nm, moreover maximal value of the induced field is much smaller in comparison with a bulk crystal. This phenomenon is caused by the vicinity of the bottom grounded electrode screening induced electric fields. From an experimental point this means that the discussed phenomena are less pronounced in the thin films ( $<500$  nm), than in the bulk plates.

The obtained experimental and theoretical results explain the abnormal switching dynamics mentioned above. In the case of the abnormal switching [12, 15, 19], the electric field induced in the tip is due to the injection of the screening charges. In the case of backswitching with formation of the ring-shaped domains [18, 21–23], it is due to the charged domain walls of the nonthrough domain.

The results of the analytical and numerical calculations demonstrate existence of the switching conditions under the grounded SPM tip. We continue to discuss the detailed mechanism of the chain formation along the tip trajectory, as opposed to continuous switching of the lines.

First, we consider the process of polarization reversal in detail. In ferroelectrics it can be considered as the first order phase transition, thus the domain kinetics is achieved through formation of nuclei and their growth [31]. The electric field averaged over the volume of the order of nucleus size (so-called “local electric field”  $E_{\text{loc}}$ ) determines the nucleation probability. The local electric field being the driving force of all nucleation processes is spatially inhomogeneous and time dependent. In general, the expression for the polar  $E_{\text{loc}}$  can be



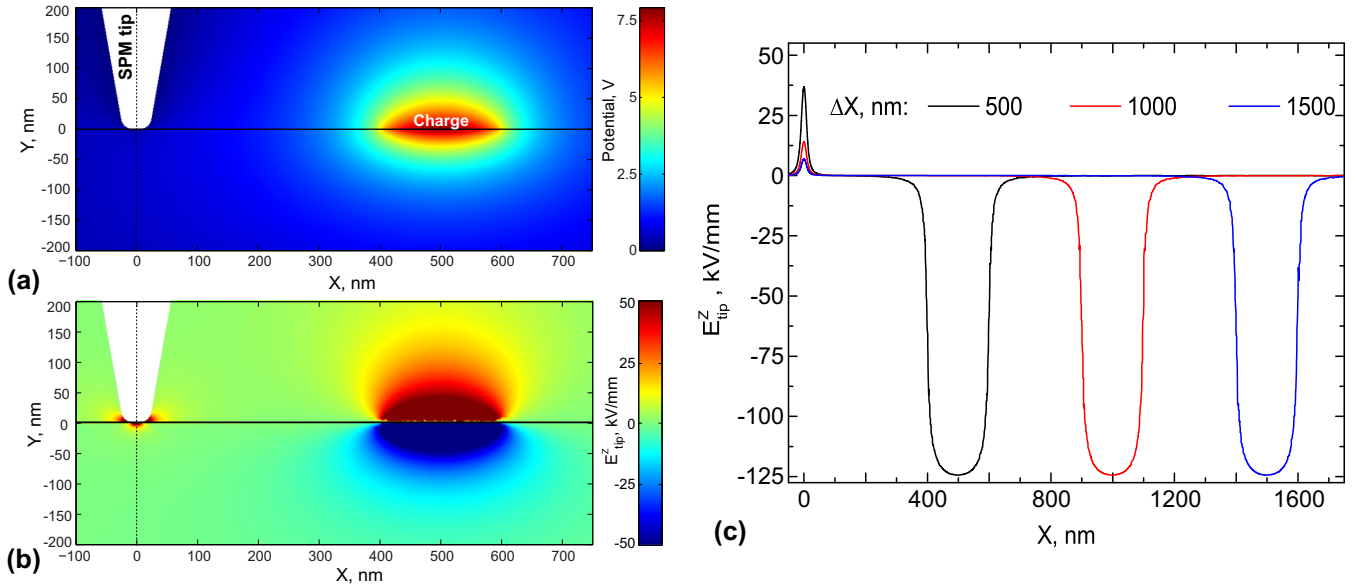


FIG. 4. (Color online) COMSOL simulations of the electric field induced by the grounded SPM tip in vicinity of the charged disk located on the surface of the anisotropic dielectric sample. Spatial distribution of the (a) electric potential and (b)  $z$  component of the electric field. (c)  $z$  component of the electric field along the line  $z = -5$  nm;  $y = 0$  nm calculated for different positions  $\Delta X$  of the charged disk on the sample surface. Simulated sample thickness is  $1 \mu\text{m}$ .

written in the following form:

$$E_{\text{loc}}(r, t) = E_{\text{ex}}(r, t) + E_{\text{dep}}(r, t) + E_{\text{scr}}(r, t), \quad (1)$$

where  $E_{\text{tip}}$  is the external electric field, produced by the tip,  $E_{\text{dep}}$  is the depolarization electric field produced by the bound charges on the polar surfaces, and  $E_{\text{scr}}$  is the screening electric field produced by the charge carriers on the sample surface (external screening) and in the sample bulk (bulk screening).

It was experimentally shown that the external screening never compensates  $E_{\text{dep}}$  completely [31], while screening by the bulk processes can take seconds [27,30]. Existence of the residual depolarization field  $E_{\text{rd}} = E_{\text{dep}} - E_{\text{scr}}$  can be attributed to the gradient of the spontaneous polarization near

the surface which can be taken into consideration by including an effective uniform surface dielectric layer (“dielectric gap” or “dead layer”) [32–35]. An effective dielectric layer of thickness  $H$  appears on the ferroelectric surface in the uniform approximation; and its “effective” dielectric properties, determined as the average values, could be different from the ferroelectric bulk [Fig. 6 (a)].

The next step to understanding the abnormal switching phenomena is to consider not a single charged disk, but a cylindrical or conic domain, with the top face covered by a sluggish screening charge. Corresponding analytical calculations of the depolarization field caused by the flat domain wall–surface junction, cylindrical domain–surface junction, and conic (or wedge) domain–surface junction allowing for the effective dielectric layer are listed in the Appendix. Approximate analytical expression for the electric field near the domain

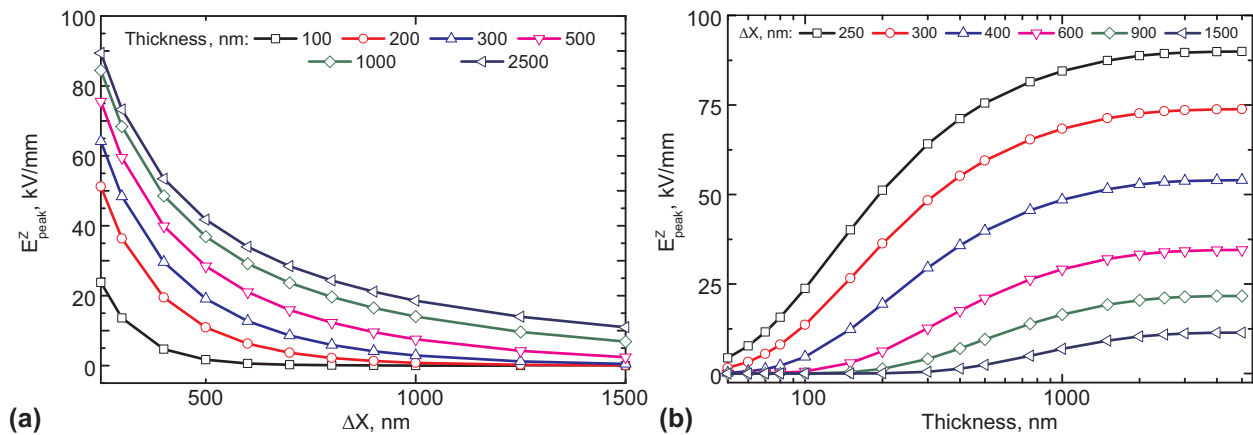


FIG. 5. (Color online) Peak value of the electric field produced by the grounded SPM tip as a function of the (a) distance to center of the charged disk  $\Delta X$  and (b) thickness of the sample.

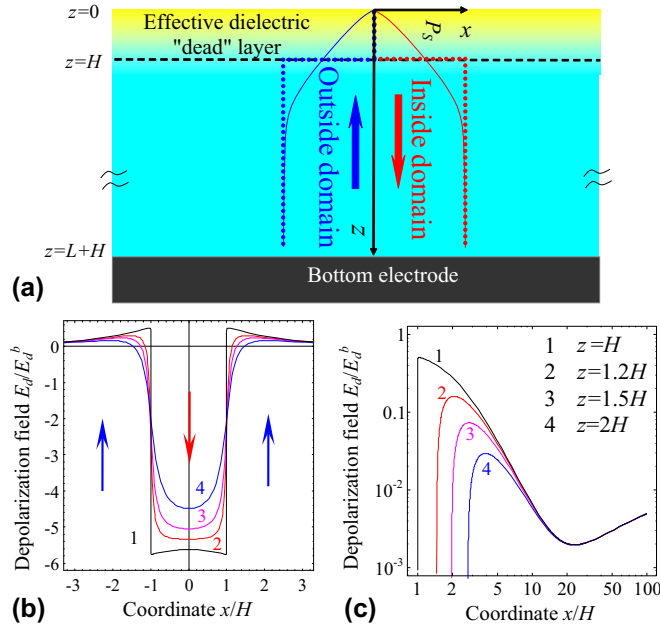


FIG. 6. (Color online) (a) Model of the effective dielectric layer. Gradient distributions of spontaneous ferroelectric polarization  $P_S(z)$  in a single-crystal region and inside a domain are shown by solid blue and red curves correspondingly. Steplike approximation used for a depolarization field calculation is shown by dotted blue and red curves correspondingly. Effective dielectric layer of thickness  $H$  appears in the approximation. (b) and (c) X profile of the z component of the depolarization field produced by conical domain with radius  $r = H$  and length  $l = 100H$  at different depths,  $z/H = 1, 1.2, 1.5, 2$  (curves 1–4). Film thickness  $L = 100H$ .  $E_d^b = P_S/(\epsilon_0\epsilon_{33}) \sim 2 \times 10^4$  kV/cm.

wall is

$$E_z(x, z) \approx -\frac{P_S}{\pi\epsilon_0\epsilon_{zz}}\{f[x, (z-H)/\gamma] - f[x, (z-H)/\gamma + 2H]\}, \quad (2)$$

where the function

$$f(x, y) = \arctan\left[\cot\left(\frac{\pi y}{2(L/\gamma + H)}\right) \tanh\left(\frac{\pi x}{2(L/\gamma + H)}\right)\right],$$

$z > H$ ,  $\gamma$  is a dielectric anisotropy factor, and  $L$  is a ferroelectric sample thickness.

Figures 6(b) and 6(c) demonstrate the spatial inhomogeneous distribution of  $E_{rd}$  in the vicinity of the prolate conic (in fact almost cylindrical near the top surface) domain wall. One can see that the field is depolarizing inside the domain and polarizing outside it.  $E_{rd}$  hampers switching right near the wall, and supports it at a distance about the thickness of the dielectric gap  $H$ . Since the bare field  $E_d^b \sim 2 \times 10^4$  kV/cm, one can conclude from Fig. 6(c) that the field calculated at depth  $z \geq H$  and lateral distances from the domain wall  $R < |x| < 2H$  can be much higher than the coercive field  $E_{th} \sim 21$  kV/mm measured experimentally in examined samples of  $\text{LiNbO}_3$ . This explains experimentally observed growth of the domain chains with the period comparable with the layer thickness  $H$  (correlated nucleation) [31].

In conclusion, we have experimentally studied the process of the tip-induced polarization reversal in the vicinity of a flat domain wall in a thin periodically poled  $\text{LiNbO}_3$  single crystal. The investigations showed nontrivial polarization switching along the path of the grounded SPM tip in the vicinity of the freshly flipped domains. The switching led to the formation of sharp spikes on the initial flat domain wall and nanodomain chains. This behavior was ascribed to the interaction between the slow dynamics of the screening charges affected both by the ferroelectric domain state and the electrostatics of the tip-surface system. Analytical and numerical calculations demonstrated the presence of an electric field produced by the charges induced into the tip surface. Formation of the nanodomain chains was explained by correlated nucleation caused by the local spatial inhomogeneity of the residual depolarization electric field.

The observed switching by the grounded SPM tip explains a number of the abnormal switching dynamics reported recently by scientific groups worldwide, including switching against an applied electric field and backswitching under the tip. Moreover, it is important for understanding of the experimental results acquired by all electrical SPM techniques realized in samples with surface and bulk charges.

This manuscript has been authored by UT-Battelle, LLC, under Contract No. DE-AC0500OR22725 with the U.S. Department of Energy. A portion of this research (A.V.I, S.V.K.) was conducted at the Center for Nanophase Materials Sciences, which is a DOE Office of Science User Facility. The equipment of the Ural Center for Shared Use “Modern nanotechnology” UrFU was used. V.Y.S. acknowledges CNMS user proposal, Ministry of Education and Science RF (UID RFMEFI59414X0011), RFBR (13-02-01391-a, 14-02-90447 Ukr-a). A.N.M acknowledges National Academy of Sciences of Ukraine (Grant 35-02-15).

#### APPENDIX: CALCULATIONS OF ELECTRIC FIELDS CREATED BY FERROELECTRIC DOMAIN WALLS–SURFACE JUNCTION ALLOWING FOR EFFECTIVE DIELECTRIC LAYER

Let us consider a thick ferroelectric single-crystal plate of thickness  $L$  that is placed on the earthed ideal electrode. Due to the gradient effects [33,34,36] polarization properties continuously change under the surface [see Fig. 6(a), solid curves]. Consequently a strong depolarization field appears.

Steplike approximation for polarization distribution can be used only for depolarization field calculations [32]. The approximation is shown by dotted curves in Fig. 6(a). An effective dielectric layer of thickness  $H$  appears on the ferroelectric surface in the approximation; its dielectric properties (determined as the average value) could be different from the ones of ferroelectric bulk. So that the background dielectric permittivity tensor of the layer is regarded as isotropic and its diagonal components are equal to  $\epsilon_e$ . Background permittivity of ferroelectric is isotropic and equal to  $\epsilon_b$ .

Going ahead we notice that the effective layer appearance can explain the scale of correlated nucleation of domains, that is about 100–500 nm, but its gradient structure (deteriorated, but still present piezoelectric properties) does not affect

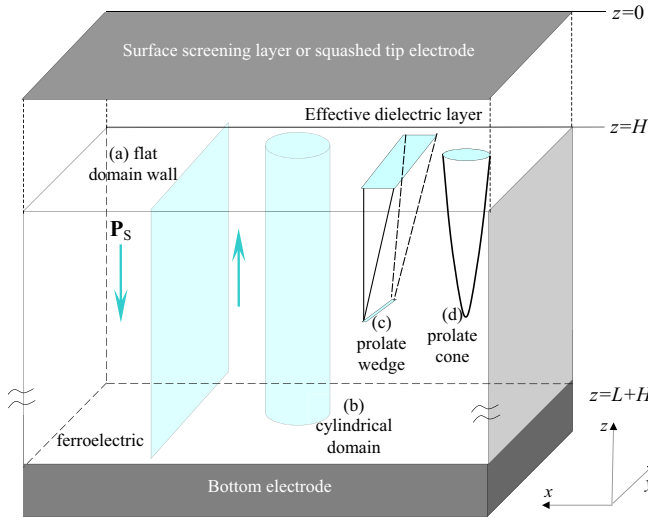


FIG. 7. (Color online) Capacitor geometry.  $\mathbf{P}_0(x, y, z)$  is spontaneous polarization and  $\mathbf{E}_f$  is the electric field inside the ferroelectric. Dotted line indicates the moving boundary of the  $180^\circ$ -domain wall. The normal vector  $\mathbf{n}$  is pointed from media 1 to media 2.

qualitatively the PFM response lateral resolution that is determined by the tip apex curvature  $\sim 15\text{--}30\text{ nm}$ .

Note that due to the effects of “reflections” in the bottom electrode this asymmetric system is equivalent to a symmetric capacitor with two dead and screening charge layers and the thickness of the ferroelectric doubled [37]. In this description it is implicitly assumed that the conductivities of the electron and hole layers are comparable.

Equations of state relate electrical displacement  $D$  and electric field  $E$  in the effective layer (subscript  $g$ ) and in ferroelectric layer (subscript  $f$ ) as

$$\mathbf{D}_g = \varepsilon_0 \varepsilon_g \mathbf{E}_g, \quad (\text{A1})$$

$$\mathbf{D}_f = \varepsilon_0 \mathbf{E}_f + \mathbf{P} \approx \varepsilon_0 \hat{\varepsilon}_{ij}^f \mathbf{E}_f + \mathbf{P}_S(x, y, z, t). \quad (\text{A2})$$

Here  $\mathbf{P}(x, y, z)$  is a polarization vector,  $\mathbf{P}(x, y, z) = (0, 0, P_S(x, y, z))$  is a spontaneous polarization vector, pointed either along or opposite the polar axis  $z$  and depending on coordinates  $x, y, z$  and time  $t$  allowing for the domain

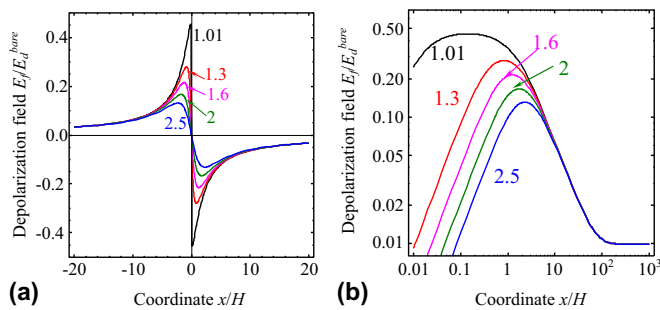


FIG. 8. (Color online) Lateral distribution ( $x$  dependence) of the depolarization field at different depths,  $z/H = 1.01, 1.3, 1.6, 2, 2.5$  (numbers near the solid curves) calculated from Eq. (A8b). Other parameters are  $\varepsilon_{33}^f \approx \gamma \varepsilon_g$  and  $L/H = 100$ . The electric field is normalized on the value  $E_d^{\text{bare}} = P_S/(\varepsilon_0 \varepsilon_{33}^f)$ .

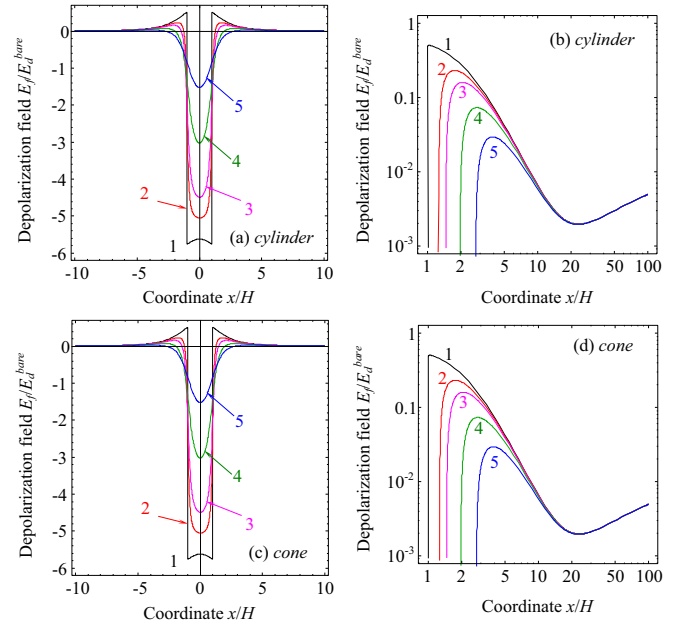


FIG. 9. (Color online) Lateral distribution ( $x$  dependence) of the depolarization field  $z$  component for the cylinder (a) and (b) and cone (c) and (d) shaped domains with radius  $R/H = 1$  and length  $h/H = 100$  at different depths,  $z/H = 1, 1.1, 1.2, 1.5, 2$  (curves 1–5). Other parameters are  $\varepsilon_{33}^f \approx \gamma \varepsilon_g$  and  $L/H = 100$ . (b) and (d) Asymptotic behavior far from domain in the log-log scale.

wall motion. For a flat  $180^\circ$ -deg domain wall and cylindrical domain [shown in Figs. 7(a) and 7(b)]  $\text{div} \mathbf{P}_S(x, y) = 0$  inside a ferroelectric, but not for the case shown in Figs. 7(c) and 7(d).

The electrostatic quasistationary Maxwell equation  $\text{rot} \mathbf{E} = 0$  should be valid. Below we introduce the potential  $\phi$  of quasistationary electric field  $\mathbf{E}_{g,f}(x, z, t) = -\nabla \phi_{g,f}(x, z, t)$ . Inside the dielectric gap potential  $\phi$  satisfies Laplace’s equation. Thus, Maxwell equation  $\text{div} \mathbf{D} = 0$  along with Eqs. (A1) and (A2) lead to

$$\left( \frac{\partial^2}{\partial z^2} + \frac{\partial^2}{\partial y^2} + \frac{\partial^2}{\partial x^2} \right) \phi_g = 0, \quad \text{for } 0 < z < H, \quad (\text{A3})$$

$$\begin{aligned} & \left[ \varepsilon_{33}^f \frac{\partial^2}{\partial z^2} + \varepsilon_{11}^f \left( \frac{\partial^2}{\partial x^2} + \frac{\partial^2}{\partial y^2} \right) \right] \phi_f \\ & = \frac{1}{\varepsilon_0} \frac{\partial P_S}{\partial z}, \quad \text{for } H < z < H + L. \end{aligned} \quad (\text{A4})$$

Equations (A3) and (A4) are supplemented with the boundary conditions of fixed top and bottom electrode potentials, continuous potential, and normal component of displacement on the boundaries between dielectric and ferroelectric layers, namely,

$$\phi_g(z=0) = 0, \quad \phi_g(z=H) = \phi_f(z=H), \quad (\text{A5})$$

$$\phi_f(z=L+H) = 0,$$

$$\begin{aligned} D_{fn} - D_{gn} &= -\varepsilon_{33}^f \frac{\partial \phi_f(x, z=H)}{\partial z} + \frac{P_{Sn}(x, y)}{\varepsilon_0} \\ &+ \varepsilon_g \frac{\partial \phi_g(x, z=H)}{\partial z} = 0. \end{aligned} \quad (\text{A6})$$

Here we consider the case of the 180-deg domain wall, in which case the wall shape is invariant in space. This approximation is justified given that shape fluctuations in the  $z$  directions are associated with significant depolarization

fields [38]. The fluctuations in the longitudinal direction and front stability will be addressed elsewhere.

For a flat 180-deg domain wall and cylindrical domain the normal component of the “depolarization” electric field has the form

$$E_{g3}(x, y, 0 < z < H) = \int_{-\infty}^{+\infty} dk_x dk_y \frac{\exp(-i k_x x - i k_y y)}{2\pi \epsilon_0} \frac{\gamma \tanh(k L / \gamma) \cosh(k z) \tilde{P}_S(k_x, k_y)}{\epsilon_{33}^f \sinh(k H) + \gamma \epsilon_g \tanh(k L / \gamma) \cosh(k H)}, \quad (\text{A7a})$$

$$E_{f3}(x, y, z > H) = \int_{-\infty}^{+\infty} dk_x dk_y \frac{\exp(-i k_x x - i k_y y)}{2\pi \epsilon_0} \frac{-\tilde{P}_S(k_x, k_y) \tanh(k H) \cosh[k(L + H - z)/\gamma]}{\epsilon_{33}^f \cosh(k L / \gamma) \tanh(k H) + \gamma \epsilon_g \sinh(k L / \gamma)}. \quad (\text{A7b})$$

Here  $\gamma = \sqrt{\epsilon_{33}^f / \epsilon_{11}^f}$  is the dielectric anisotropy factor,  $k = \sqrt{k_x^2 + k_y^2}$ , and  $\tilde{P}_S(k_x, k_y, t)$  is the Fourier image of  $P_S(x, y)$  over coordinates  $x, y$ . Complete screening of the field inside the ferroelectric is achieved for zero thickness of the effective dielectric layer ( $H = 0$ ) by the free charges on the top electrode.

For the particular case of the flat 180-deg domain wall [Eq. (A7b)] we are interested in, it can be simplified as

$$E_{f3}(x, z > H) = \int_{-\infty}^{+\infty} dk_x \frac{\exp(-i k_x x)}{2\pi \epsilon_0} \frac{-\tilde{P}_S(k_x) \tanh(k_x H) \cosh[k_x(L + H - z)/\gamma]}{\epsilon_{33}^f \cosh(k_x L / \gamma) \tanh(k_x H) + \gamma \epsilon_g \sinh(k_x L / \gamma)}. \quad (\text{A8a})$$

Using that  $\tilde{P}_S(k_x) = \frac{i\pi L_\perp P_S}{\sinh(\pi k_x L_\perp)}$  for a flat single domain wall profile,  $\tilde{P}_S(k_x) = P_S \tanh(\frac{x}{2L_\perp})$  in the second order ferroelectrics, where  $L_\perp$  is the domain wall width. For CLN  $L_\perp \sim 1$  nm at room temperature. Neglecting the width of the domain wall  $L_\perp \rightarrow 0$  and supposing that  $\epsilon_{33}^f \approx \gamma \epsilon_g$  we derived the exact expression:

$$E_3(x, z > H) \approx -\frac{P_S}{\epsilon_0 \epsilon_{33}^f} \frac{1}{\pi} \left( \arctan \left[ \cot \left( \frac{\pi(z - H)/\gamma}{2(L/\gamma + H)} \right) \tanh \left( \frac{\pi x}{2(L/\gamma + H)} \right) \right] - \arctan \left[ \cot \left( \frac{\pi[(z - H)/\gamma + 2H]}{2(L/\gamma + H)} \right) \tanh \left( \frac{\pi x}{2(L/\gamma + H)} \right) \right] \right). \quad (\text{A8b})$$

Accuracy of Eq. (A8b) against Eq. (A8a) is rather high at  $L_\perp \ll H$  (e.g., at  $L_\perp \sim 1$  nm). Equation (A8b) [as well as (A8a) in the sense of principal value] contains the limit at  $x \gg H$ :

$$E_3(x \rightarrow \pm\infty, z > H) \approx \frac{\mp P_S H}{\epsilon_0 (\epsilon_{33}^f H + \epsilon_g L)}. \quad (\text{A8c})$$

Note that for a thickness  $H \sim 100$  nm a depolarization field is still essential at distances  $\sim 10 H \sim 1000$  nm [Figs. 8(a) and 8(b)]. Thus the domain-wall interaction (and consequently correlated nucleation) mediated by the  $\sim 100$  nm effective dielectric layer naturally becomes extremely long range.

For the particular case of the *cylindrical domain* Eq. (A7b) can be simplified as

$$E_{f3}(\rho, z > H) = \int_0^{+\infty} dk k \frac{J_0(k\rho)}{\epsilon_0} \frac{-\tilde{P}_S(k) \tanh(k H) \cosh[k(L + H - z)/\gamma]}{\epsilon_{33}^f \cosh(k L / \gamma) \tanh(k H) + \gamma \epsilon_g \sinh(k L / \gamma)}. \quad (\text{A9a})$$

The particular case of the cylindrical domain is shown in Figs. 9(a) and 9(b) for  $z/H = 1-2$ . Here we used the following Fourier image of polarization distribution:

$$\tilde{P}_S(k_x, k_y) = -P_S \delta(k_x) \delta(k_y) 2\pi + 2P_S R J_1(kR)/k. \quad (\text{A9b})$$

Here  $R$  is the domain radius. Note that the more complex shape of the domain radius  $R$  should be  $z$  dependent (and so a more complex expression for depolarization field should be used, see below).

For the particular case of the *prolate domain* with  $\frac{\partial P_S}{\partial z} \neq 0$ , Eq. (A7b) should be modified as

$$E_{f3}(\rho, z > H) = \int_0^{+\infty} dk k J_0(k\rho) \tilde{E}_{3f}(k, z, t), \quad (\text{A10a})$$

where we used Fourier image

$$\begin{aligned} \tilde{E}_{3f}(\mathbf{k}, z > H) = & -\frac{\tilde{P}_S(\mathbf{k}, z)}{\epsilon_0 \epsilon_{33}^f} + \frac{k}{\gamma} \left( \int_H^z d\xi \frac{\cosh[k(\xi - H)/\gamma] \cosh[k(L + H - z)/\gamma]}{\sinh(kL/\gamma)} \frac{\tilde{P}_S(\mathbf{k}, \xi)}{\epsilon_0 \epsilon_{33}^f} \right. \\ & + \int_z^{L+H} d\xi \frac{\cosh[k(z - H)/\gamma] \cosh[k(L + H - \xi)/\gamma]}{\sinh(kL/\gamma)} \frac{\tilde{P}_S(\mathbf{k}, \xi)}{\epsilon_0 \epsilon_{33}^f} \Big) \\ & - \int_H^{L+H} d\xi \frac{k/\gamma \cosh[k(L + H - \xi)/\gamma] \sinh(kH) \cosh[k(L + H - z)/\gamma] \tilde{P}_S(\mathbf{k}, \xi)}{\epsilon_0 [\epsilon_{33}^f \cosh(\frac{k}{\gamma}L) \sinh(kH) + \gamma \epsilon_g \cosh(kH) \sinh(\frac{k}{\gamma}L)] \sinh(kL/\gamma)}. \end{aligned} \quad (\text{A10b})$$

With polarization image

$$\tilde{P}_S(k_x, k_y, z) = -P_S \delta(k_x) \delta(k_y) 2\pi + 2P_S R(z) \frac{J_1[kR(z)]}{k}. \quad (\text{A10c})$$

In the particular case of *conic domain*

$$R(z) = R_0 \left( 1 - \frac{z - H}{h} \right) \quad \text{at } z > H \quad \text{and } z < H + h. \quad (\text{A10d})$$

Lateral distribution ( $x$  dependence) of the depolarization field  $z$  component for the cylinder and cone shaped domains with radius  $R/H = 1$  and length  $h/H = 100$  at different depth  $z/H = 1-2$  are shown in Fig. 9.

Since the bare field  $E_d^{\text{bare}} \sim 2 \times 10^4$  kV/cm, one can conclude from Figs. 8 and 9 that the electric field calculated at depth  $z = H$  and at distance from the domain wall  $H < x < 2H$  can be much higher than the threshold field  $E_c \sim 210$  kV/cm measured experimentally in examined samples of LiNbO<sub>3</sub>.

- 
- [1] O. Kolosov, A. Gruverman, J. Hatano, K. Takahashi, and H. Tokumoto, *Phys. Rev. Lett.* **74**, 4309 (1995).
- [2] A. Gruverman, O. Auciello, and H. Tokumoto, *Annu. Rev. Mater. Sci.* **28**, 101 (1998).
- [3] E. Soergel, *J. Phys. D Appl. Phys.* **44**, 464003 (2011).
- [4] S. V. Kalinin, A. N. Morozovska, L. Q. Chen, and B. J. Rodriguez, *Rep. Prog. Phys.* **73**, 056502 (2010).
- [5] Y. Cho, K. Fujimoto, Y. Hiranaga, Y. Wagatsuma, A. Onoe, K. Terabe, and K. Kitamura, *Appl. Phys. Lett.* **81**, 4401 (2002).
- [6] S. Hong, E. L. Colla, E. Kim, D. V. Taylor, A. K. Tagantsev, P. Muralt, K. No, and N. Setter, *J. Appl. Phys.* **86**, 607 (1999).
- [7] M. Abplanalp, J. Fousek, and P. Günter, *Phys. Rev. Lett.* **86**, 5799 (2001).
- [8] P. Paruch, T. Tybell, and J. M. Triscone, *Appl. Phys. Lett.* **79**, 530 (2001).
- [9] K. Terabe, S. Takekawa, M. Nakamura, K. Kitamura, S. Higuchi, Y. Gotoh, and A. Gruverman, *Appl. Phys. Lett.* **81**, 2044 (2002).
- [10] A. V. Ievlev, S. Jesse, A. N. Morozovska, E. Strelcov, E. A. Eliseev, Y. V. Pershin, A. Kumar, V. Y. Shur, and S. V. Kalinin, *Nat. Phys.* **10**, 59 (2014).
- [11] T. Morita and Y. Cho, *Appl. Phys. Lett.* **84**, 257 (2004).
- [12] S. Bühlmann, E. Colla, and P. Muralt, *Phys. Rev. B* **72**, 214120 (2005).
- [13] B. J. Rodriguez, R. J. Nemanich, A. Kingon, A. Gruverman, S. V. Kalinin, K. Terabe, X. Y. Liu, and K. Kitamura, *Appl. Phys. Lett.* **86**, 012906 (2005).
- [14] A. Agronin, M. Molotskii, Y. Rosenwaks, G. Rosenman, B. J. Rodriguez, A. I. Kingon, and A. Gruverman, *J. Appl. Phys.* **99**, 104102 (2006).
- [15] A. L. Kholkin, I. K. Bdkin, V. V. Shvartsman, and N. A. Pertsev, *Nanotechnology* **18**, 095502 (2007).
- [16] E. I. Shishkin, A. V. Ievlev, E. V. Nikolaeva, M. S. Nebogatikov, and V. Y. Shur, *Ferroelectrics* **374**, 26 (2008).
- [17] A. Wu, P. M. Vilarinho, D. Wu, and A. Gruverman, *Appl. Phys. Lett.* **93**, 262906 (2008).
- [18] M. Lilienblum and E. Soergel, *J. Appl. Phys.* **110**, 052018 (2011).
- [19] A. V. Ievlev, A. N. Morozovska, E. A. Eliseev, V. Y. Shur, and S. V. Kalinin, *Nat. Commun.* **5**, 5545 (2014).
- [20] J. Guyonnet, E. Agoritsas, S. Bustingorry, T. Giamarchi, and P. Paruch, *Phys. Rev. Lett.* **109**, 147601 (2012).
- [21] Y. Kim, S. Bühlmann, S. Hong, S. H. Kim, and K. No, *Appl. Phys. Lett.* **90**, 072910 (2007).
- [22] J. Woo, S. Hong, N. Setter, H. Shin, J.-U. Jeon, Y. E. Pak, and K. No, *J. Vac. Sci. Technol. B* **19**, 818 (2001).
- [23] J. Woo, S. Hong, D. K. Min, H. Shin, and K. No, *Appl. Phys. Lett.* **80**, 4000 (2002).
- [24] Y. Kim, J. Kim, S. Bühlmann, S. Hong, Y. K. Kim, S.-H. Kim, and K. No, *Phys. Status Solidi Rapid Res. Lett.* **2**, 74 (2008).
- [25] E. I. Shishkin, V. Y. Shur, O. Mieth, L. M. Eng, L. L. Galambos, and R. O. Miles, *Ferroelectrics* **340**, 129 (2006).
- [26] A. V. Ievlev, D. O. Alikin, A. N. Morozovska, O. V. Varenyk, E. A. Eliseev, A. L. Kholkin, V. Y. Shur, and S. V. Kalinin, *ACS Nano* **9**, 769 (2015).
- [27] S. Tong, W. I. Park, Y.-Y. Choi, L. Stan, S. Hong, and A. Roelofs, *Phys. Rev. Appl.* **3**, 014003 (2015).
- [28] S. Hong, S. Tong, W. I. Park, Y. Hiranaga, Y. S. Cho, and A. Roelofs, *Proc. Natl. Acad. Sci. USA* **111**, 6566 (2014).
- [29] Y. Kim, C. Bae, K. Ryu, H. Ko, Y. K. Kim, S. Hong, and H. Shin, *Appl. Phys. Lett.* **94**, 032907 (2009).
- [30] V. Y. Shur, A. R. Akhmatkhanov, M. A. Chuvakova, and I. S. Baturin, *Appl. Phys. Lett.* **105**, 152905 (2014).
- [31] V. Y. Shur, *J. Mater. Sci.* **41**, 199 (2006).



- [32] V. M. Fridkin, *Ferroelectric Semiconductors* (Consultant Bureau, New York, 1980).
- [33] A. N. Morozovska, E. A. Eliseev, Y. Li, S. V. Svechnikov, P. Maksymovych, V. Y. Shur, V. Gopalan, L.-Q. Chen, and S. V. Kalinin, *Phys. Rev. B* **80**, 214110 (2009).
- [34] V. R. Aravind, A. N. Morozovska, S. Bhattacharyya, D. Lee, S. Jesse, I. Grinberg, Y. L. Li, S. Choudhury, P. Wu, K. Seal, A. M. Rappe, S. V. Svechnikov, E. A. Eliseev, S. R. Phillpot, L. Q. Chen, V. Gopalan, and S. V. Kalinin, *Phys. Rev. B* **82**, 024111 (2010).
- [35] A. N. Morozovska, E. A. Eliseev, A. V. Ievlev, O. V. Varenik, A. S. Pusenkova, Y.-H. Chu, M. V. Strikha, V. Y. Shur, and S. V. Kalinin, *J. Appl. Phys.* **116**, 066817 (2014).
- [36] A. Morozovska, S. Svechnikov, E. Eliseev, B. Rodriguez, S. Jesse, and S. Kalinin, *Phys. Rev. B* **78**, 054101 (2008).
- [37] G. B. Stephenson and K. R. Elder, *J. Appl. Phys.* **100**, 051601 (2006).
- [38] G. Catalan, H. Bea, S. Fusil, M. Bibes, P. Paruch, A. Barthelemy, and J. F. Scott, *Phys. Rev. Lett.* **100**, 027602 (2008).